Longitudinal and spin-valley Hall optical conductivity in single layer MoS_2

Zhou Li[1,*] and J. P. Carbotte[1,2,†]

[1]*Department of Physics, McMaster University, Hamilton, Ontario, Canada, L8S 4M1*

[2]*Canadian Institute for Advanced Research, Toronto, Ontario, Canada M5G 1Z8*

(Received 28 August 2012; revised manuscript received 29 October 2012; published 21 November 2012)

A monolayer of MoS_2 has a noncentrosymmetric crystal structure, with spin-polarized bands. It is a two-valley semiconductor with the direct gap falling in the visible range of the electromagnetic spectrum. Its optical properties are of particular interest in relation to valleytronics and possible device applications. We study the longitudinal and the transverse Hall dynamical conductivity which is decomposed into charge, spin, and valley contributions. The circular polarized light associated with each of the two valleys separately is considered and results are filtered according to spin polarization. Temperature can greatly change the spin admixture seen in the frequency window where they are not closely in balance.

DOI: 10.1103/PhysRevB.86.205425 PACS number(s): 72.20.−i, 75.70.Tj, 78.67.−n

I. INTRODUCTION

Since the isolation of graphene,[1,2] the search for new two-dimensional atomic membranes possibly with novel functionalities has intensified. MoS_2 (Ref. 3) in its single-layered form is a two-valley direct band-gap semiconductor with the gap in the visible regime and so it is of interest for device applications. Through excitation by the right- and left-hand polarized light, excess populations of a selected valley can be generated which make this material ideal for valleytronics.[4–7] Because the two inequivalent valleys are separated in the Brillouin zone by a large momentum, intervalley scattering should be small. Consequently, the valley index becomes a new degree of freedom analogous to spin in semiconductors. Just like manipulating spin has lead to spintronics,[8,9] manipulating the valley index can produce new effects including using it to carry information. As an example, in the context of graphene Xiao *et al.*[10] showed that a contrasting intrinsic magnetic moment and Berry curvature can be associated with the carrier valley index. As a second example a valley filter device was described by Rycerz *et al.*.[11]

An important issue is the possible pathways to achieve valley polarization (i.e., populating states preferentially in one valley[12]). One way discussed theoretically[4,10,13,14] was to use circular polarized light, which was demonstrated recently by three experimental groups.[5–7,12] Selection rules on the absorption of right-handed (or left-handed) polarized light assures that this radiation excites almost exclusively the charge carriers residing in a single valley with index $\tau = +1$ (or -1). The physical quantity that comes into the description of such processes is the real part of the ac optical conductivity for right $(+1)$ or left (-1) polarization $\mathrm{Re}\sigma_{\pm}$ as a function of photon energy ω. In terms of the longitudinal $\sigma_{xx}(\omega)$ and transverse $\sigma_{xy}(\omega)$ conductivity $\sigma_{\pm}(\omega) \equiv \sigma_{xx}(\omega) \pm i\sigma_{xy}(\omega)$. The conductivity also plays an important role in determining the optical properties of nanostructures as we can see from Refs. 15–20. To solve the Maxwell equations for systems with a graphene sheet between two media with different dielectric constants, one has to know the conductivity of two-dimensional graphene. The results for the conductivity of single-layer MoS_2 will be useful if similar devices were built from MoS_2 instead of graphene.

MoS_2 is a layer of molybdenum atoms between two layers of sulfur in a trigonal prismatic arrangement which does not have inversion symmetry. In momentum space at the K and $-K$ points of the honeycomb lattice[21,22] the valence and conduction bands are separated by a large semiconductor direct band-gap Δ (Ref. 23) and there is a large spin-orbit coupling leading to a spin polarization of the valence band, spin up $\uparrow$ and down $\downarrow$ as the z component of the spin operator s_z commutes with the Hamiltonian and hence remains a good quantum number. A minimal Hamiltonian which describes the band structure of MoS_2 (valid near the main absorption edge) is found in Ref. 4 with parameters based on first-principles calculations for the group-VI dichalcogenides.[21,24] A more complete theory is found in Ref. 14 where a calculation of the dc Hall conductivity and Berry curvature over the entire Brillouin zone is presented. Part of the Hamiltonian describes the dynamics of massive Dirac fermions which are known from the graphene literature to have an optical response quite different from that of an ordinary two-dimensional (2D) electron gas. For example, a universal constant background conductivity of $e^2/(4\hbar)$ (Refs. 25 and 26) [for a single spin and single valley this constant becomes $e^2/(16\hbar)$] is predicted and observed for photon energy ω greater than twice the chemical potential μ for massless Dirac fermions. We use this Hamiltonian to calculate the dynamic optical conductivity as a function of photon energy to several electron volts. The results are presented for longitudinal $\sigma_{xx}(\omega)$ as well as transverse conductivity $\sigma_{xy}(\omega)$, which is separated in charge, spin, and valley Hall conductivity. Appropriate contributions from different spin channels are presented separately and special attention is payed to the effects of right- and left-handed light polarization. Temperature effects are also considered. In Sec. II we present the Hamiltonian and the Green's function on which our calculations are based. In Sec. III the mathematical expressions for the conductivity are evaluated and results for spin and valley Hall conductivity are given for several representative values of the chemical potential. The results for circular polarized light are found in Secs. IV and V contains a summary.

II. FORMALISM

The Hamiltonian for MoS_2 at K and $-K$ points is

$$H_0 = at(\tau k_x \hat{\sigma}_x + k_y \hat{\sigma}_y) + \frac{\Delta}{2}\hat{\sigma}_z - \lambda\tau\frac{\hat{\sigma}_z - 1}{2}\hat{S}_z, \quad (1)$$

with 2λ the spin-orbit splitting at the top of the valence band and we take $2\lambda = 0.15\,\text{eV}$, a the lattice parameter 3.193 Å, t the hopping $t = 1.1\,\text{eV}$, $\hat{\sigma}$ the Pauli matrices, and $\hat{S}_z$ the spin matrix for the z component of spin s_z, which is a good quantum number here. The index $\tau = \pm 1$ is the valley $K(-K)$, respectively, and Δ is the direct band gap equal to 1.66 eV between the valence and conduction bands. The x and y velocity components based on Eq. (1) are

$$v_x = \frac{\partial H_0}{\hbar \partial k_x} = \frac{at}{\hbar}\tau\sigma_x, \quad v_y = \frac{\partial H_0}{\hbar \partial k_y} = \frac{at}{\hbar}\sigma_y. \tag{2}$$

Here we will be interested in the charge, spin, and valley current given, respectively, as $\mathbf{j} = e\mathbf{v}$,$\mathbf{j}^s = \frac{\hbar}{2}s_z\mathbf{v}$, and $\mathbf{j}^v = \tau\mathbf{v}$. The eigenenergies and vectors of Eq. (1) are

$$E_k^{\pm}(\tau, s_z) = \lambda\tau s_z/2 \pm \sqrt{a^2t^2k^2 + \left(\frac{\Delta'}{2}\right)^2} \tag{3}$$

and

$$u_n(k) = \frac{atk\left(1, \frac{-\Delta'/2 \pm \sqrt{a^2t^2k^2 + (\Delta'/2)^2}}{at}\frac{\tau k_x + ik_y}{k^2}\right)^T}{\sqrt{a^2t^2k^2 + (-\Delta'/2 \pm \sqrt{a^2t^2k^2 + (\Delta'/2)^2})^2}} \tag{4}$$

with $\Delta' = \Delta - \lambda\tau s_z$ (Ref. 27). For later reference, the Berry curvature for the conduction band E_k^+ is

$$\begin{aligned}\Omega_c(k) &= z \cdot \nabla_k \times \langle u_n(k)|i\nabla_k|u_n(k)\rangle \\ &= -\tau\frac{2a^2t^2\Delta'}{[\Delta'^2 + 4a^2t^2k^2]^{3/2}}\end{aligned} \tag{5}$$

with valence band $\Omega_v(k) = -\Omega_c(k)$. With these solutions the Green's function $\hat{G}_0(\mathbf{k}, i\omega_n)$ with Matsubara frequencies ω_n is

$$\begin{aligned}&\hat{G}_0(\mathbf{k}, i\omega_n) \\ &= \frac{(i\hbar\omega_n + \mu - \lambda\tau s_z/2)\hat{I} + \left(\frac{\Delta'}{2}\right)\hat{\sigma}_z + at(\tau k_x\sigma_x + k_y\sigma_y)}{(i\hbar\omega_n + \mu - \lambda\tau s_z/2)^2 - a^2t^2k^2 - \left(\frac{\Delta'}{2}\right)^2} \\ &\equiv G_1(\mathbf{k}, i\omega_n)\hat{I} + G_z\hat{\sigma}_z + G_x\hat{\sigma}_x + G_y\hat{\sigma}_y,\end{aligned} \tag{6}$$

which gives

$$\begin{aligned}G_1(\mathbf{k}, i\omega_n) &= \frac{1}{2}\frac{1}{i\hbar\omega_n + \mu - \lambda\tau s_z/2 - \sqrt{a^2t^2k^2 + \left(\frac{\Delta'}{2}\right)^2}} \\ &\quad + \frac{1}{2}\frac{1}{i\hbar\omega_n + \mu - \lambda\tau s_z/2 + \sqrt{a^2t^2k^2 + \left(\frac{\Delta'}{2}\right)^2}}, \\ G_z &= \frac{\frac{\Delta'}{2}}{(i\hbar\omega_n + \mu - \lambda\tau s_z/2)}G_1(\mathbf{k}, i\omega_n), \\ G_x &= \frac{at\tau k_x}{(i\hbar\omega_n + \mu - \lambda\tau s_z/2)}G_1(\mathbf{k}, i\omega_n), \\ G_y &= \frac{atk_y}{(i\hbar\omega_n + \mu - \lambda\tau s_z/2)}G_1(\mathbf{k}, i\omega_n).\end{aligned} \tag{7}$$

The density of state $N(\epsilon)$ is given by

$$N(\epsilon) = -\frac{1}{\pi}\sum_{\mathbf{k}}\text{Im}G_1(\mathbf{k}, i\omega_n -> \epsilon + i\delta), \tag{8}$$

where $\sum$ is a sum over momentum, Im means taking the imaginary part. The longitudinal conductivity $\sigma_{xx}(\omega)$, charge Hall conductivity $\sigma_{xy}(\omega)$, spin Hall conductivity $\sigma_{xy}^s(\omega)$, and valley Hall conductivity $\sigma_{xy}^v(\omega)$ are given by[28–30]

$$\begin{aligned}&\sigma_{xx}(\omega) = -\frac{e^2a^2t^2}{i\omega\hbar^2}T\sum_{\mathbf{k},l} \\ &Tr\langle\sigma_x G_0(\mathbf{k}, i\omega_l)\sigma_x G_0(\mathbf{k}, i\omega_l + i\omega_n)\rangle_{i\omega_n -> \omega + i\delta} \\ &\sigma_{xy}(\omega) = -\frac{e^2a^2t^2}{i\omega\hbar^2}T\sum_{\mathbf{k},l}, \\ &\text{Tr}\langle\tau\sigma_x G_0(\mathbf{k}, i\omega_l)\sigma_y G_0(\mathbf{k}, i\omega_l + i\omega_n)\rangle_{i\omega_n -> \omega + i\delta}, \\ &\sigma_{xy}^s(\omega) = -\frac{ea^2t^2}{i\omega\hbar^2}T\sum_{\mathbf{k},l}, \\ &\text{Tr}\left\langle\frac{\hbar}{2}s_z\tau\sigma_x G_0(\mathbf{k}, i\omega_l)\sigma_y G_0(\mathbf{k}, i\omega_l + i\omega_n)\right\rangle_{i\omega_n -> \omega + i\delta}, \\ &\sigma_{xy}^v(\omega) = -\frac{ea^2t^2}{i\omega\hbar^2}T\sum_{\mathbf{k},l}, \\ &\text{Tr}\langle\sigma_x G_0(\mathbf{k}, i\omega_l)\sigma_y G_0(\mathbf{k}, i\omega_l + i\omega_n)\rangle_{i\omega_n -> \omega + i\delta}.\end{aligned} \tag{9}$$

After simplification we get

$$\sigma_{xy}(\omega) = -\frac{e^2}{\hbar^2}\sum_{\mathbf{k},\tau,s_z}\Omega_c(k)[f(E^+) - f(E^-)]g, \tag{10a}$$

with

$$g \equiv \frac{(4a^2t^2k^2 + \Delta'^2)}{(\hbar\omega + i\delta)^2 - (4a^2t^2k^2 + \Delta'^2)} \tag{10b}$$

for the spin and valley Hall conductivities, g in Eq. (10b) is to be replaced by $s_z g/e$ and $\tau g/e$, respectively. Here $f(x)$ is the Fermi Dirac function, which contains the chemical potential μ. The longitudinal conductivity is

$$\begin{aligned}\sigma_{xx}(\omega) = \frac{e^2}{\hbar^2}\sum_{\mathbf{k},\tau,s_z}&\frac{2a^2t^2\left(4a^2t^2k_y^2 + \Delta'^2\right)}{i\omega[\Delta'^2 + 4a^2t^2k^2]^{1/2}} \\ &\times\frac{[f(E^+) - f(E^-)]}{(\hbar\omega + i\delta)^2 - (4a^2t^2k^2 + \Delta'^2)}.\end{aligned} \tag{10c}$$

To obtain Eq. (10c) we have included only the interband transitions. There is an additional intraband contribution which provides a delta function contribution at $\omega = 0$. When residual scattering is included in the calculations, the intraband piece broadens into a Drude peak which can overlap with the interband contribution. But in the pure limit, which is the case we are considering here, we need not consider this contribution. What replaces the Berry curvature in the expression for the longitudinal conductivity σ_{xx} is a factor

$$h \equiv -\frac{2a^2t^2\left(4a^2t^2k_y^2 + \Delta'^2\right)}{i\omega[\Delta'^2 + 4a^2t^2k^2]^{3/2}} \tag{10d}$$

For $k = 0$ this factor in σ_{xx} and σ_{xy} agrees and as we will see later this leads to a valley selection rule for circular polarized light; at finite k, however, the cancellation is no longer exact.

III. RESULTS FOR SPIN AND VALLEY HALL CONDUCTIVITY

In Fig. 1 we show our results for the Hall conductivity $\sigma_{xy}(\omega)$ vs. $\hbar\omega$ in units of $e/\hbar$ for the four values of the chemical potential shown in the inset of the top frame where the band energies $E_k^{\pm}(\tau, s_z)$ are sketched [Eq. (3)]. $\mu = -0.995$ eV falls below the top of the lowest energy spin-polarized valence band; $\mu = -0.845$ eV falls between the two valence bands. $\mu = 0.09$ eV is between the valence and conduction bands (insulator) while $\mu = 0.92$ eV falls in the conduction band also spin split, but this splitting is small. In the main frame

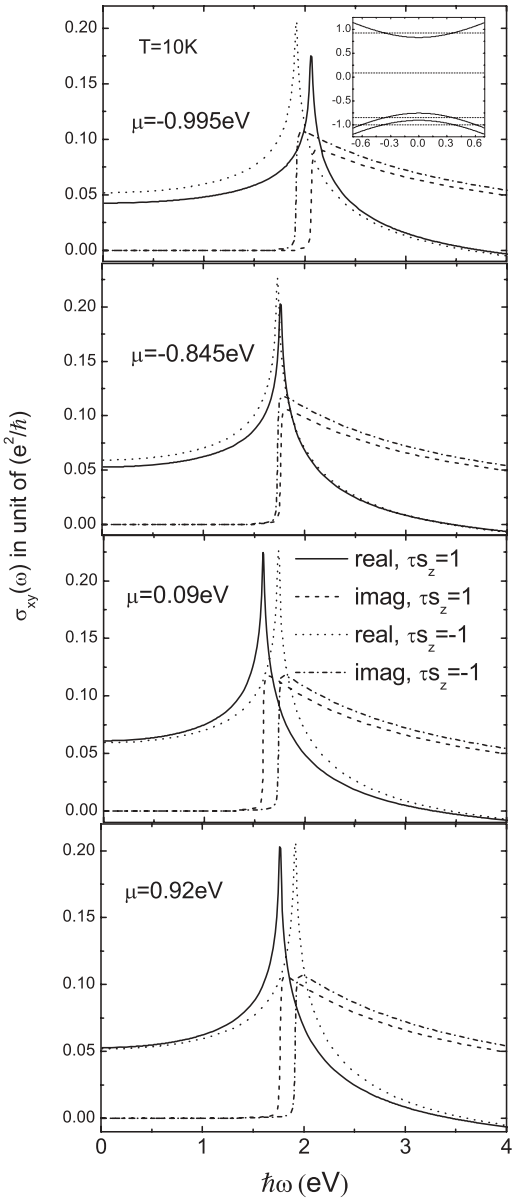

FIG. 1. Real (solid) part of the Hall conductivity σ_{xy} vs. ω, and its imaginary part (dashed) for $\tau s_z = 1$. The dotted and dashed dotted curves are for $\tau s_z = -1$ instead. There are 4 frames from top to bottom for four values of chemical potential μ namely -0.995, -0.845,0.09 and 0.92 eV respectively. The inset provides a sketch of the bands in MoS_2 and how the four values of μ relate to these. In all cases the bands are cut off at momentum $ka = 3.0$.

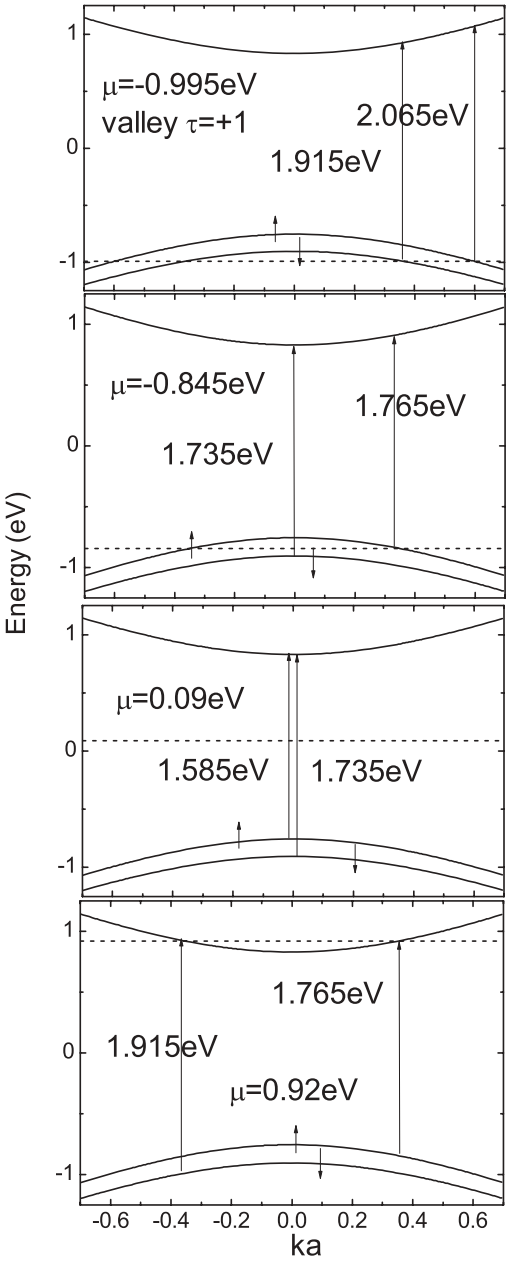

FIG. 2. The energy bands (solid) for MoS_2 with chemical potential μ level indicated by a dashed horizontal line. The extremal optical transitions are also indicated in each case. From top to bottom frame $\mu = -0.995, -0.845, 0.09$ and $0.92\,eV$.

which has four frames each for a different value of μ we show separately the contribution for $\tau s_z = \pm 1$ with $\sigma_{xy}(\omega)$ the sum over both the index s_z(spin) and τ (valley). The solid line is the real part for $\tau s_z = 1$ while for $\tau s_z = -1$ the dotted line applies. The dashed and dash-dotted lines are for their respective imaginary parts. We note a sharp onset in these two last curves, the energy of which can be traced to the minimum energy associated with the possible interband optical transition as shown in Fig. 2. As an example, in the top frame we see that, for $\mu = -0.995$ eV, the onset of the interband transitions for spin $\uparrow$ occurs at higher energies than for spin $\downarrow$ (here the valley index has been taken to be 1). Corresponding to the onset in Imσ_{xy} there is a peak in its real part at this same energy

as they are related by the Kramers-Kronig relations. The results presented were obtained through numerical evaluation of Eq. (10a). The numerical values do have some dependence on the cutoff used on the energy $(atk)^2$. Here we have set the cutoff ak to be 3 and restrict ourselves to photon energies below 3 eV. In this energy range choosing a larger cutoff makes no difference to the results which have converged. For photon energies above 3 eV, a range not considered explicitly in our figures, increasing the cutoff even to infinity has no qualitative effect on the results for the imaginary part of $\sigma_{xy}(\omega)$. It affects the real part more. With a cutoff, there is a zero in $\mathrm{Re}\sigma_{xy}(\omega)$ at some high energy. As the cutoff is increased, the energy of the zero in $\mathrm{Re}\sigma_{xy}(\omega)$ moves to higher energies and in the limit of infinite cutoff no zero remains for finite ω as it has moved to infinity. Taking the infinite band limit has the advantage that simple analytic expressions can be obtained, which can be useful. For example, it is straight forward to show that

$$\mathrm{Im}\sigma_{xy}(\omega) = -\frac{e^2}{16\hbar}\frac{2(\Delta-\lambda)}{\hbar\omega}\theta[\hbar\omega-(\Delta-\lambda)] \times\left[f\left(\frac{\lambda}{2}+\frac{\hbar\omega}{2}-\mu\right)-f\left(\frac{\lambda}{2}-\frac{\hbar\omega}{2}-\mu\right)\right], \tag{11}$$

where we have made explicit the value of the chemical potential attached to the thermal function $f(x)$ [the Fermi Dirac distribution $f(x)\equiv 1/(e^{\beta x}+1)$ with $\beta = 1/T$]. Note the onset at $(\Delta-\lambda)$ and the $1/\omega$ drop in this function as a function of ω. While there are some quantitative differences of the form (11) with our numerical results there are no qualitative changes. Another reason for restricting the range of photon energies considered, as we have done here, is that the model Hamiltonian (1) is itself valid only near the main absorption edge. A first-principles calculation of the dc Hall conductivity and Berry curvature over the entire Brillouin zone which goes beyond what we have done is given by Feng *et al.*.[14] Here we really cannot access accurately the high-energy region.

To get the spin and valley Hall conductivity from the results presented in Fig. 1 components need to be added according to the weighting of $\hbar s_z/(2e)$ and τ/e, respectively, as noted in relation to Eq. (10a). The results are presented in Fig. 3. The real part of the valley Hall conductivity is the solid curve with the dashed line the corresponding imaginary part, while the dotted and dashed-dotted lines are for the spin Hall conductivity. The differences in weighting s_z and τ have a large effect on the resulting Hall conductivity. For example, the real part of the valley Hall conductivity is everywhere positive in our model while the spin Hall conductivity starts negative at $\omega = 0$ and is very small in comparison to the valley Hall conductivity. Both show peaks at the onset energies associated with their imaginary part. Because of the spin splitting of our bands there are two peaks seen clearly in the real part of the valley Hall conductivity (solid curve), after which it drops off gradually with increasing ω. Consequently, the real part of the spin Hall conductivity (dotted curve) changes sign with increasing ω because the two peaks found in Fig. 1 (solid and dotted curves) are associated with opposite spin, this sign-changing behavior has also been found in the Fig. 4(a) of Ref. 14. While the results show quantitative variations with

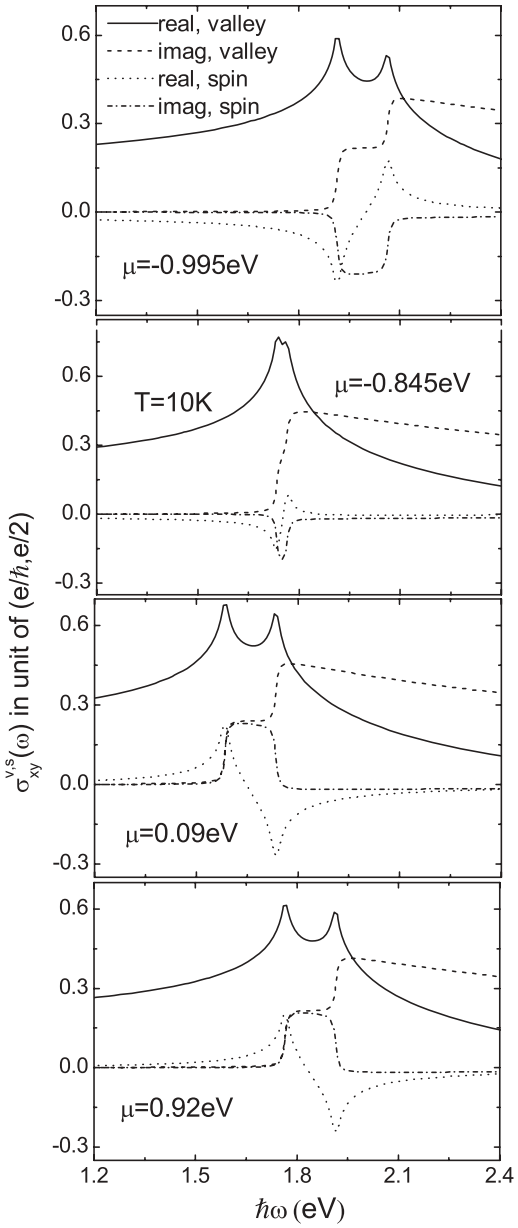

FIG. 3. The real (solid) and imaginary (dashed) parts of the valley Hall conductivity σ_{xy} vs. ω. The dotted and dashed-dotted curves are similar results for the spin Hall conductivity case. From top to bottom frame the chemical potentials $\mu = -0.995, -0.845, 0.09$, and 0.92 eV. The inset in Fig. 1 provides a sketch of the bands in MoS_2 and how the four values of μ relate to these.

the value chemical potential (see inset in Fig. 1), there is no qualitative change.

The zero energy limit ($\omega = 0$) of the Hall conductivity is of interest and can be worked out analytically in the infinite band limit. At zero temperature ($T = 0$) the results are (σ_{xy}^s in unit of $\frac{e}{2}$, σ_{xy}^v in unit of $\frac{e}{\hbar}$)

$$\sigma_{xy}^s(\omega=0) = \frac{\lambda}{\pi}\frac{\Delta-2\mu}{\lambda^2-4\mu^2}, \tag{12a}$$

$$\sigma_{xy}^v(\omega=0) = \frac{1}{\pi}\frac{2\mu\Delta-\lambda^2}{\lambda^2-4\mu^2} \tag{12b}$$

for μ in the lowest valence band;

$$\frac{1}{2\pi}\frac{\Delta-2\lambda+2\mu}{\lambda-2\mu} \quad \text{and} \quad \frac{1}{2\pi}\frac{\Delta-2\mu}{\lambda-2\mu} \tag{12c}$$

for μ between the $\uparrow$, $\downarrow$ valence band;

$$0 \quad \text{and} \quad \frac{1}{\pi} \tag{12d}$$

for μ between the valence and conduction bands and

$$\frac{\lambda}{\pi}\frac{\Delta-2\mu}{4\mu^2-\lambda^2} \quad \text{and} \quad \frac{1}{\pi}\frac{2\mu\Delta-\lambda^2}{4\mu^2-\lambda^2} \tag{12e}$$

for μ above the conduction band. Note in particular for μ between the valence and conduction bands $\sigma^s_{xy}(\omega=0)=0$ and $\sigma^v_{xy}(\omega=0)=\frac{e}{\pi\hbar}$. Here we do not have a spin Hall insulating state. Note that for the real part of the Hall conductivity at zero temperature an analytical expression exists, for example, for $\tau=1, s_z=1$,

$$\mathrm{Re}\sigma_{xy}(\omega) = -\frac{e^2}{8\pi\hbar^2\omega}(\Delta-\lambda) \times \ln\left|\frac{\hbar\omega-2\sqrt{x_{\min}}}{\hbar\omega+2\sqrt{x_{\min}}}\frac{\hbar\omega+2\sqrt{x_{\max}}}{\hbar\omega-2\sqrt{x_{\max}}}\right| \tag{13a}$$

with

$$x_{\min} = \max\left[\left(\mu-\frac{\lambda}{2}\right)^2, \left(\frac{\Delta-\lambda}{2}\right)^2\right] \tag{13b}$$

$$x_{\max} = (ka)^2_{\mathrm{cut}}t^2 + \left(\frac{\Delta-\lambda}{2}\right)^2. \tag{13c}$$

$(ka)_{\mathrm{cut}}$ is the cutoff for ka in the infinite band approximation $(ka)_{\mathrm{cut}}\to\infty$ while in our numerical results $(ka)_{\mathrm{cut}}=3.0$. Similar results can be found, for example, in Ref. 31.

IV. CIRCULAR POLARIZED LIGHT AND TEMPERATURE EFFECT

For circular polarized light the appropriate optical conductivity is

$$\sigma_{\pm}(\omega) \equiv \sigma_{xx}(\omega) \pm i\sigma_{xy}(\omega), \tag{14}$$

where the longitudinal and charge Hall conductivities given by Eqs. (10a) and (10c). The results for the absorptive part of the conductivity $\mathrm{Re}\sigma_{\pm}(\omega)$ are presented in Fig. 4 where we show separately $\mathrm{Re}\sigma_{xx}$ (solid curve) for $s_z=+1$ and (dotted curve) for $s_z=-1$, to be compared with the dashed curve for $\mathrm{Im}\sigma_{xy}$ with $s_z=+1$ and dash-dotted curve for $s_z=-1$. For a given spin the onset in each pair of curves for longitudinal and Hall conductivities are the same. The two begin to deviate from each other as ω is increased above the threshold where the Hall conductivity falls below its longitudinal value.

For the infinite band case we have seen in Eq. (11) that $\mathrm{Im}\sigma_{xy}$ drops like $1/\omega$. Similar algebra for the infinite band

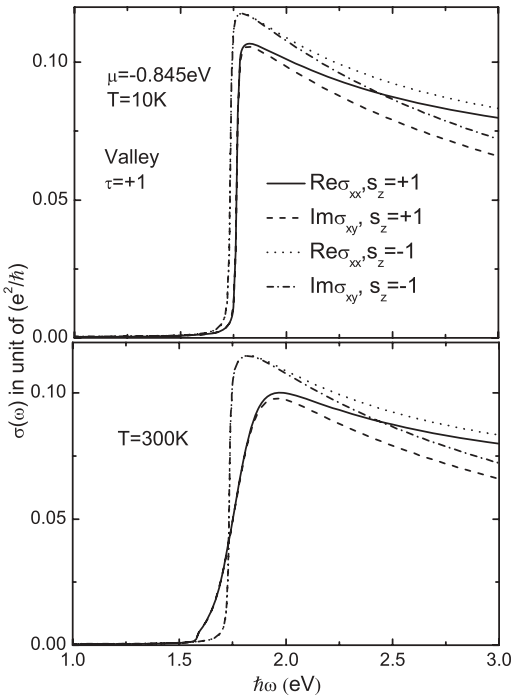

FIG. 4. The absorptive part of the longitudinal [$\mathrm{Re}\sigma_{xx}(\omega)$] and transverse Hall conductivity [$\mathrm{Im}\sigma_{xy}(\omega)$] as a function of photon energy ω. The chemical potential is $\mu=-0.845$ eV. The top frame is for temperature $T=10$ K and the bottom for $T=300$ K. The solid and dashed curves are for $\mathrm{Re}\sigma_{xx}(\omega)$ and $\mathrm{Im}\sigma_{xy}(\omega)$ with $\tau=+1$ (valley index) and $s_z=+1$ (spin index), while the dotted and dashed-dotted curves are for $s_z=-1$.

limit gives for the longitudinal conductivity

$$\mathrm{Re}\sigma_{xx}(\omega) = -\frac{e^2}{16\hbar}\left[1+\frac{(\Delta-\lambda)^2}{\hbar^2\omega^2}\right]\theta[\hbar\omega-(\Delta-\lambda)] \times\left[f\left(\frac{\lambda}{2}+\frac{\hbar\omega}{2}-\mu\right)-f\left(\frac{\lambda}{2}-\frac{\hbar\omega}{2}-\mu\right)\right], \tag{15}$$

which drops less rapidly with increasing ω than does $\mathrm{Im}\sigma_{xy}(\omega)$ in Eq. (11) and provides a check in our numerical results shown in Fig. 4 for a finite cutoff $ka=3$.

The results in the top frame of Fig. 4 apply to temperature $T=10$ K, while those in the bottom are for $T=300$ K. For the specific value of μ chosen (i.e., $\mu=-0.845$ eV) the chemical potential falls between the two spin-polarized valence bands. On comparison with the top frame we note considerable temperature smearing of the spin-up band. But the spin-down band by comparison is much less affected as it does not fall at the Fermi energy, but is everywhere below μ and hence does not respond to temperature as effectively.

In Fig. 5 we present our results for $\mathrm{Re}\sigma_{\pm}(\omega)$ vs. ω in units of $e^2/\hbar$ for valley $\tau=-1$ in the case $\mu=-0.845$ eV. The top frame applies to $T=10$ K while the temperature is 300 K in the bottom frame. The results are presented separately for $s_z=\pm1$. We note that $\mathrm{Re}\sigma_{+}(\omega)$ is large and comparable in size for either spin up or down while $\mathrm{Re}\sigma_{-}(\omega)$ is very small in comparison. This is understood from the optical selection rule which applies to σ_{xx} and σ_{xy}. In the infinite band limit we can

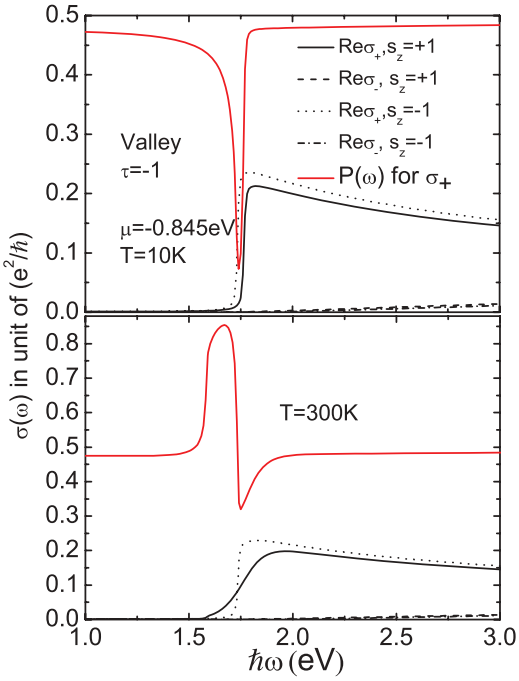

FIG. 5. (Color online) Results for the absorptive part of the conductivity for circularly polarized light $\sigma_{\pm}(\omega) \equiv \sigma_{xx} \pm i\sigma_{xy}$. Here the valley index $\tau = -1$. The solid curve is for $\mathrm{Re}\sigma_{+}$ and the dashed curve for $\mathrm{Re}\sigma_{-}$, both for spin index $s_z = +1$. For $s_z = -1$ the dotted curve is σ_{+} and the dashed-dotted curve for σ_{-}. The dominant response in this valley is from σ_{+} right-handed circular polarization, also shown on the same figure is the up to up plus down spin polarization for σ_{+} (solid red curve). The top frame is at $T = 10\,\mathrm{K}$ and the bottom at $T = 300\,\mathrm{K}$.

show that

$$\mathrm{Re}\sigma_{xx}(\omega) \mp \mathrm{Im}\sigma_{xy}(\omega) = -\frac{e^2}{16\hbar}\theta[\hbar\omega - (\Delta - \lambda)] \times \left[1 \pm \frac{(\Delta - \lambda)}{\hbar\omega}\right]^2 \left[f\left(\frac{\lambda}{2} + \frac{\hbar\omega}{2} - \mu\right) - f\left(\frac{\lambda}{2} - \frac{\hbar\omega}{2} - \mu\right)\right], \quad (16)$$

which implies a perfect cancellation at the onset energy $\omega = (\Delta - \lambda)$. Here Eq. (16) is for the $s_z = +1$ band with $-\lambda \to \lambda$ for the $s_z = -1$ case. Effectively, light polarization provides valley selection to a very good approximation. It is exact at the onset energy and remains quite good even at $\omega = 4\,\mathrm{eV}$, for which energy the light polarization will reduce the absorption from this valley to about 20% its value for the opposite polarization. The polarization selection rule found here for the dynamical conductivity agrees fully with those previously discussed by Yao *et al.*[13] for the inversion symmetry-breaking Hamiltonian in two valley systems, where they related the optical selection rule to the orbital magnetic moment and the Berry curvature of the particular valley considered. It is interesting to look at the spin-up spin-down admixture of the optical response $\mathrm{Re}\sigma_{+}(\omega)$ vs. ω. We define

$$P(\omega) = \frac{\sigma_{+}^{\text{spin up}}(\omega)}{\sigma_{+}^{\text{spin up}}(\omega) + \sigma_{+}^{\text{spin down}}(\omega)}. \quad (17)$$

The results are shown as the red curve in Fig. 5. We note that for most frequencies $P(\omega)$ is close to $1/2$, but that around the onset energy for σ_{+} there is a region where $P(\omega)$ falls below this value and can be close to 0. This is easily understood as a direct consequence of the displacement in the onset between $\mathrm{Re}\sigma_{+}(\omega)$ for spin down (dotted curve) and for spin up (solid curve), which implies a deficit of the spin-up electron in the region between these two onsets. Temperature can have a large effect on the position and shape of $P(\omega)$ in the region of the onset as seen in the lower frame of Fig. 5. This can be traced to the fact that the spin-up electrons are much more susceptible to temperature smearing for the case considered here, as we have already noticed. The solid curve ($\uparrow$) for σ_{+} now extends to lower energies than does the short dashed curve ($\downarrow$). Temperature can in fact change the magnitude of $P(\omega)$ in the region of interest from less than $1/2$ to larger than $1/2$ with this entire region shifted toward lower energies. The peak in $P(\omega)$ for $T = 300\,\mathrm{K}$ is also broadened as compared with the valley in this same quantity for $T = 10\,\mathrm{K}$. The spin admixture in this region can be manipulated with temperature.

V. SUMMARY AND CONCLUSION

We present expressions for the dynamic conductivity of MoS_2 based on a simplified Hamiltonian which includes spin-orbit coupling and band-structure parameters fit to first-principles calculations. Using the Kubo formula, the final expressions reduce to a sum over momentum k centered about the two valley points K and $-K$ defining the corners of the honeycomb lattice in the Brillouin zone. The bands are spin polarized and a sum over the spin and valley appears. The transverse conductivity is split into charge, spin, and valley Hall conductivity and, in all cases, depends on an overlap of the Berry curvature multiplied with a common sum of two energy denominators linear in frequency plus the appropriate temperature factors and channel-dependent indices. The expression for the longitudinal conductivity is not quite as simple but reduces to the common form around $k = 0$ (zero momentum). Simplified analytic expressions can be obtained in the infinite band limit. We present numerical results for all these quantities as a function of photon energy separating out, in each case, the contribution from the separate spin channels. In the numerical calculations we use a cutoff on momentum of $ka = 3.0$. The results are not qualitatively different from the infinite band case although there are important quantitative differences. The effect of temperature is considered. It provides a smearing that tends to obscure the separate contributions to the conductivity. It also can change very significantly the spin admixture in the frequency window just above the main absorption threshold where there can be an important imbalance between the up and down spins, for a given valley when circular polarized light is employed. The absorptive part of the conductivity for right- and left-handed polarized light, which is the appropriate quantity for valleytronics, is also computed, and it is found that the second valley contributes very little to the absorption. For example, it is less than 20% at $\omega = 4\,\mathrm{eV}$, with the main absorption peak at 1.7 eV. The dc limit of the Hall conductivities is obtained analytically. For the parameters appropriate to MoS_2, the real part of the valley Hall conductivity is positive and large in value

as compared to its spin Hall counterpart, which is negative for some values of the chemical potential. We hope that our calculations can help further our understanding of the optical properties of MoS_2.

ACKNOWLEDGMENTS

This work was supported by the Natural Sciences and Engineering Research Council of Canada (NSERC) and the Canadian Institute for Advanced Research (CIfAR).

*lizhou@univmail.cis.mcmaster.ca
†carbotte@univmail.cis.mcmaster.ca

[1] K. S. Novoselov, A. K. Geim, S. V. Morozov, D. Jiang, Y. Zhang, S. V. Dubonos, I. V. Grigorieva, and A. A. Firsov, Science **306**, 666 (2004).
[2] X. Zhang, Y.-W. Tan, H. L. Stormer, and P. Kim, Nature (London) **438**, 201 (2005).
[3] K. S. Novoselov, D. Jiang, F. Schedin, T. J. Booth, V. V. Khotkevich, S. V. Morozov, and A. K. Geim, Proc. Natl. Acad. Sci. USA **102**, 10451 (2004).
[4] D. Xiao, G. B. Liu, W. Feng, X. Xu, and W. Yao, Phys. Rev. Lett. **108**, 196802 (2012).
[5] H. Zeng, J. Dai, W. Yao, D. Xiao, and X. Cui, Nat. Nanotechnol. **7**, 490 (2012).
[6] K. F. Mak, K. He, J. Shan, and T. F. Heinz, Nat. Nanotechnol. **7**, 494 (2012).
[7] T. Cao, G. Wang, W. Han, H. Ye, C. Zhu, J. Shi, Q. Niu, P. Tan, E. Wang, B. Liu, and J. Feng, Nat. Commun. **3**, 887 (2012).
[8] S. A. Wolf, D. D. Awschalom, R. A. Buhrman, J. M. Daughton, S. von Molnar, M. L. Roukes, A. Y. Chtchelkanova, and D. M. Treger, Science **294**, 1488 (2001).
[9] J. Fabian, A. Matos-Abiague, C. Ertler, P. Stano, and I. Zutic, Acta Physica Slovaca **57**, 565 (2007).
[10] D. Xiao, W. Yao, and Q. Niu, Phys. Rev. Lett. **99**, 236809 (2007).
[11] A. Rycerz, J. Tworzydło, and C. W. J. Beenakker, Nat. Phys. **3**, 172 (2007).
[12] K. Behnia, Nat. Nanotechnol. **7**, 488 (2012).
[13] W. Yao, D. Xiao, and Q. Niu, Phys. Rev. B **77**, 235406 (2008).
[14] W. Feng, Y. Yao, W. Zhu, J. Zhou, W. Yao, and D. Xiao, Phys. Rev. B. **86**, 165108 (2012).
[15] M. Jablan, H. Buljan, and M. Soljacic, Phys. Rev. B. **80**, 245435 (2009).
[16] A. Y. Nikitin, F. Guinea, F. J. Garcia-Vidal, and L. Martin-Moreno, Phys. Rev. B. **84**, 195446 (2011).
[17] Ashkan Vakil and Nader Engheta, Science **332**, 1291 (2011).
[18] F. Koppens, D. E. Chang and F. J. García de Abajo, Nano Lett. **11**, 3370 (2011).
[19] J. Chen *et al.*, Nature **487**, 77 (2012).
[20] Z. Fei *et al.*, Nature **487**, 82 (2012).
[21] Z. Y. Zhu, Y. C. Cheng, and U. Schwingenschlögl, Phys. Rev. B **84**, 153402 (2011).
[22] T. Li and G. Galli, J. Phys. Chem. C **111**, 16192 (2007).
[23] K. F. Mak, C. Lee, J. Hone, J. Shan, and T. F. Heinz, Phys. Rev. Lett. **105**, 136805 (2010).
[24] T. Cheiwchanchamnangij and W. R. L. Lambrecht, Phys. Rev. B **85**, 205302 (2012).
[25] A. H. Castro Neto, F. Guinea, N. M. R. Peres, K. S. Novoselov, and A. K. Geim, Rev. Mod. Phys. **81**, 109 (2009).
[26] V. N. Kotov, B. Uchoa, V. M. Pereira, F. Guinea and A. H. Castro Neto, Rev. Mod. Phys. **84**, 1067 (2012).
[27] For silicene, a simpler Hamiltonian applies for which the linear term in the energy $E_k^{\pm}(\tau, s_z)$ of Eq. (3) is missing. The issues of interest and the parameters used are also quite different. See L. Stille, C. J. Tabert, and E. J. Nicol, Phys. Rev. B **86**, 195405 (2012).
[28] V. P. Gusynin, S. G. Sharapov, and J. P. Carbotte, Phys. Rev. Lett. **96**, 256802 (2006).
[29] E. J. Nicol and J. P. Carbotte, Phys. Rev. B **77**, 155409 (2008).
[30] T. Stauber and N. M. R. Peres, J. Phys. Conds. Matt. **20**, 055002 (2008).
[31] W. K. Tse and A. H. MacDonald, Phys. Rev. Lett. **105**, 057401 (2010).